The Meteoritical Society

Meteoritics & Planetary Science 43, Nr 1/2, 215–231 (2008)
Abstract available online at http://meteoritics.org

Recovering the elemental composition of comet Wild 2 dust in five Stardust impact tracks and terminal particles in aerogel

Hope A. ISHII[1*], Sean BRENNAN[2], John P. BRADLEY[1], Katharina LUENING[2], Konstantin IGNATYEV[2], and Piero PIANETTA[2]

[1]Institute for Geophysics and Planetary Physics, Lawrence Livermore National Laboratory, Livermore, California 94550, USA
[2]Stanford Synchrotron Radiation Laboratory, Stanford Linear Accelerator Center, Menlo Park, California 94025, USA
[*]Corresponding author. E-mail: hope.ishii@llnl.gov

(Submitted 10 January 2007; revision accepted 27 June 2007)

Abstract–The elemental (non-volatile) composition of five Stardust impact tracks and terminal particles left from capture of comet 81P/Wild 2 dust were mapped in a synchrotron X-ray scanning microprobe with full fluorescence spectra at each pixel. Because aerogel includes background levels of several elements of interest, we employ a novel "dual threshold" approach to discriminate against background contaminants: an upper threshold, above which a spectrum contains cometary material plus aerogel and a lower threshold below which it contains only aerogel. The difference between normalized cometary-plus-background and background-only spectra is attributable to cometary material. The few spectra in-between are discarded since misallocation is detrimental: cometary material incorrectly placed in the background spectrum is later subtracted from the cometary spectrum, doubling the loss of reportable cometary material. This approach improves accuracy of composition quantification. We present the refined whole impact track and terminal particle elemental abundances for the five impact tracks. One track shows mass increases in Cr and Mn (1.4×), Cu, As and K (2×), Zn (4×), and total mass (13%) by dual thresholds compared to a single threshold. Major elements Fe and Ni are not significantly affected. The additional Cr arises from cometary material containing little Fe. We exclude Au intermixed with cometary material because it is found to be a localized surface contaminant carried by comet dust into an impact track. The dual threshold technique can be used in other situations where elements of interest in a small sample embedded in a matrix are also present in the matrix itself.

INTRODUCTION AND MOTIVATION

Stardust, a NASA Discovery class mission, returned to Earth nearly one year ago with dust captured from the coma of comet 81P/Wild 2 (or simply Wild 2) (Brownlee et al. 2003, Brownlee et al. 2006a). Microscopic dust grains were captured at a relative velocity of 6.1 km/s in passive collectors comprised of low-density silica aerogel tiles and aluminum foils covering the aerogel holder frame (Tsou et al. 2003). These Stardust samples have a unique status in our collections of extraterrestrial materials: They are the first samples returned from a known parent body that originated in the Kuiper belt beyond the gas giants. Prior to 1974, Wild 2 orbited at heliocentric distances beyond Jupiter, but a gravitational encounter with that planet sent it into a short-period orbit in the inner solar system (Sekanina and Yeomans 1985; Królikowska and Szutowicz 2006) and allowed the Stardust spacecraft to intercept the comet's coma within the orbit of Mars. Since comet Wild 2 is a newcomer to the inner solar system and not yet altered by repeated exposure to the Sun's heat and radiation, the collected dust offers an historic view into the nature of Kuiper belt objects. It is expected that most small bodies in the frozen Kuiper belt have experienced little thermal or aqueous processing since formation and are therefore relatively unaltered since the solar system formed about 4.6 billion years ago (Irvine and Lunine 2004).

Stardust particles can now be compared in terms of elemental and isotopic composition, organics and mineralogy with other primitive extraterrestrial materials available on Earth including meteorites, micrometeorites, and interplanetary dust particles. Our focus is on the elemental chemistry of Stardust particles measured by synchrotron X-ray fluorescence. Prior to the Stardust mission, cometary (non-volatile) elemental compositions were inferred from remote infrared spectroscopy and impact ionization mass spectrometry at comet 1P/Halley (Jessberger 1999) where spaceflight restrictions on instrumentation limited resolution and sensitivity. Stardust samples are now available for study by highly sensitive and

accurate ground-based instruments, e.g., synchrotrons, greatly improving the quality of composition analysis possible.

We have analyzed 5 Stardust impact tracks produced by Wild 2 dust captured in aerogel using micro-focused synchrotron X-ray fluorescence measurements (micro-SXRF). A key advantage of micro-SXRF is the ability to measure the composition of the comet sample while it is still embedded in the aerogel capture medium for reduced risk of contamination and minimal to no effect on the sample itself. These composition data may then be compared with those of other extraterrestrial samples, meteorites, and interplanetary dust particles. The 5 samples presented here were among 23 analyzed by the Preliminary Examination (PE) Team, an international collaboration in which we participated. The PE Team was tasked with providing a first look at the Stardust samples within one year of the return as a baseline for subsequent research. Initial results have been presented in several publications by the PE Team (Brownlee et al. 2006b; Flynn et al. 2006; Hörz et al. 2006; Keller et al. 2006; McKeegan et al. 2006; Sandford et al. 2006; Zolensky et al. 2006). The initial composition data from 23 Stardust impact tracks were collected and analyzed at several synchrotron sources using a variety of protocols and analysis methods with varying accuracies and precisions. We present here, in detail, the refined bulk elemental chemistry results from synchrotron X-ray microprobe micro-SXRF measurements of the 5 entire impact tracks and their terminal particles analyzed at the Stanford Synchrotron Radiation Laboratory. We also demonstrate the analytical approach we have developed in order to more effectively distinguish cometary material from aerogel matrix background for improved accuracy of composition measurements. We propose that this approach be used in future composition measurements for improved average compositions. Using this new approach, examination of one impact track revealed localized Au contamination and enabled its exclusion from cometary abundance estimates. This approach is applicable to other cases in which some elements of interest in a small sample embedded in a matrix are also present in the matrix itself.

SAMPLES AND EXPERIMENTAL METHODS

The five Stardust impact tracks in this study were provided through NASA Curation as part of the Stardust Preliminary Examination. All were extracted from the same aerogel tile, Cell 44, in the form of individual aerogel "keystones" (Westphal et al. 2004). Figure 1 shows optical micrographs of the keystones after extraction (scaled approximately to each other). Each keystone contains a single impact track, a cavity in the silica aerogel formed by the hypervelocity capture of an impacting unit or impactor. Some impactors disaggregated on impact generating multiple sub-tracks from a single entry hole, and some remained relatively intact. In either case, debris measurable by micro-SXRF is left along the track. The tracks presented here vary from approximately 0.3 to 3.3 mm in length and from conical, "carrot" shapes to more bulbous shapes. All of these tracks were found to contain terminal particles, a portion of the original impacting unit lodged at the terminus of the track. Table 1 provides a listing of the official NASA Curation sample numbers, track names as referred to in this paper, details of track length, and shape and the total and Fe mass determined by the methodology described below.

Each impact track was mapped in the hard X-ray scanning fluorescence microprobe, an end station of wiggler Beam Line 6-2 at the Stanford Synchrotron Radiation Laboratory. The microprobe uses Kirkpatrick-Baez final focusing optics and adjustable virtual source slits for a beam size of 2×2 microns^2 with 10^9 photons per second (ph/s). For efficient mapping of Stardust impact tracks, the focused spot size was increased to 15×19 microns^2 with 4×10^{10} ph/s (and 6×15 microns^2 with 2×10^{10} ph/s for Track 12). Si (111) monochromator crystals selected 14 keV incident X-rays for easy access to the K absorption edges of elements from Si through Br. The microprobe is equipped with a Leica optical microscope and aluminum-coated low-Z mirror for X-ray line-of-sight viewing and positioning of the sample in the X-ray beam. Helium is flown over the X-ray sample interaction region to reduce air absorption, ozone generation, and Ar fluorescence. Each keystone was translated in the beam in steps matched to the FWHM of the focused spot size with dwell times of 500 seconds/pixel for Track 5, 60 seconds/pixel for Track 9, and 30 seconds/pixel for all other tracks. Full fluorescence spectra were collected at each pixel. Terminal particles and other particles along tracks were located primarily by high Fe fluorescence and scatter count rates. For consistency, terminal particle data reported here were isolated from whole track maps. (Higher sensitivity particle compositions will be reported in a future publication.) An ultraclean Si(Li) detector with ~150 eV resolution (Mn Kα) collected the fluorescent X-rays in a geometry perpendicular to the incident beam in the plane of the storage ring. An ion chamber provided pre- and a PIN diode post-sample intensity measurements.

Micro-SXRF cometary and background spectra were fit using PyMca, a program developed by Dr. Armando Solé at the European Synchrotron Radiation Facility (ESRF) and available for public use (Solé et al. 2007). Whole track and terminal particle masses were derived from the difference between the sum of the on-track spectra containing cometary material and the normalized aerogel matrix background spectrum. Details of isolating pixels containing cometary material from background are discussed below. We note that large Si and significant Ar fluorescence intensities (from aerogel and air) combined with frequent high Fe fluorescence intensities from the samples produce a variety of detector-related sum peaks (for example, Ar Kα + Si Kα and Si Kα + Si Kα) and escape peaks (Fe Kα – Si Kα) that complicate peak-fitting of low intensity peaks in the low atomic number (Z) element range between S and Ti. The effect

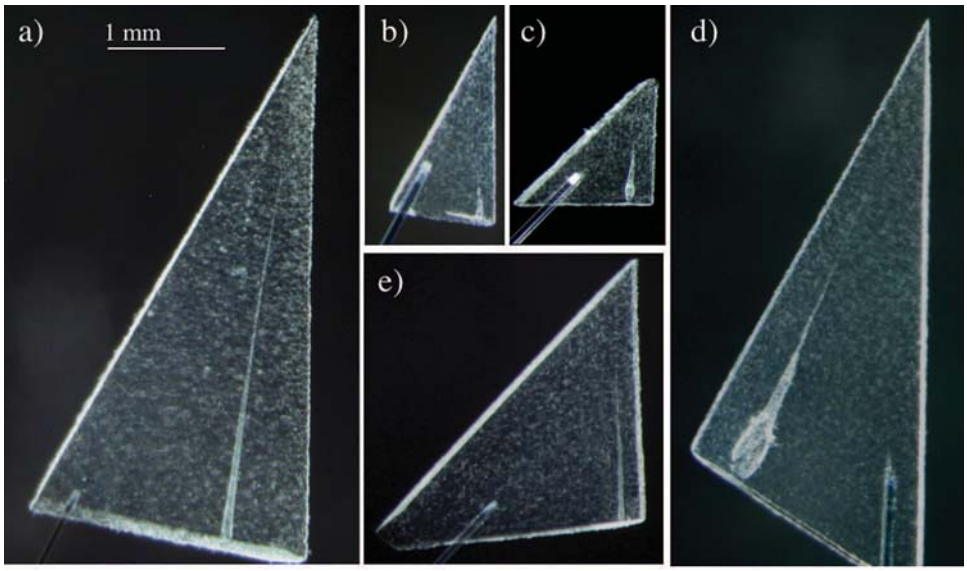

Fig. 1. Optical microscope images of the 5 Stardust comet dust impact tracks in aerogel keystones analyzed by micro-SXRF: a) Track 4, b) Track 5, c) Track 9, d) Track 10, and e) Track 12. Images are scaled to indicate relative sizes of tracks. See Table 1 for details of impact track length and mass of cometary debris.

Table 1. The five Stardust impact tracks analyzed by micro-synchrotron X-ray fluorescence.[a]

NASA sample #	Nickname	Track length (mm)[b]	Shape	Total measured mass (ng)	Total Fe mass (ng)	Terminal particle/whole track (Fe mass%)
C2044,0,39	Track 5	0.3	Bulb	0.046	0.012	2.05%
C2044,0,42	Track 9	0.5	Bulb	0.135	0.112	6.12%
C2044,0,52	Track 12	1.6	Carrot	0.404	0.298	29.99%
C2044,0,43	Track 10	2.8	Bulb	2.347	2.142	9.28%
C2044,0,38	Track 4	3.3	Carrot	1.375	1.228	32.65%
				4.307	3.793	

[a]Each comet dust impact track is identified by NASA Curation sample number, nickname used in the present work, approximate length, shape, measured total and Fe masses and the percent of Fe mass in the terminal particle. While this final value may be an indication of the differences in dispersion of mass along the impact track with track shape, it is important to note that the micro-SXRF measurements do not include the mass of Si, O, Mg, Al, or C in the cometary material, and forsterite and enstatite terminal particles dominated by Si and O have frequently been found in Stardust impacts (Zolensky et al. 2006).

[b]Approximate, determined optically.

on fitted peak area can be significant: For Ca, neglecting to fit sum and escape peaks may introduce an error of as much as 20%.

We note that other sources of error include background subtraction under the spectra, both cometary material spectra and aerogel matrix spectra. A variety of effects, including incomplete charge collection, lead to a spectral background with composition-dependent shape. We have used PyMCA algorithms; however, it is not possible to subtract an exact background without full iterative modeling of fluorescence and detector response. Errors from this source will impact most strongly those elements with low abundance in the cometary material relative to the aerogel. No attempt has been made to quantify this error source at present.

Two reference standards were employed in quantifying element masses: a thin (64 nm) Fe film acted as an absolute reference standard, and a USGS basaltic glass microprobe standard[1] NKT-1G thin section (200 nm) was used to determine the energy-dependent correction for elements below Fe. Typical thin film standards contain about 1 wt% Fe; however, bulk average extraterrestrial materials can be expected to contain Fe levels near solar levels of about 18 wt%. Because the NKT-1G basaltic glass standard contains about 9.5 wt% Fe, this correction provides partial compensation for self-absorption of low-Z fluorescence X-rays (for example, sulfur) and corrects for detector response. Without detailed knowledge of sample geometry, densities, and composition, this self-absorption correction is necessarily coarse; however, we find that particle sizes in these tracks, measured by the Fe fluorescence, are always less than or equal to 5 microns. As a result, self-absorption will be small for elements above Ca, and mass precisions are generally 20% or better for elements above Ca. Statistical uncertainty is ≤10% (by mass) for all elements

[1]Results of the G-Probe-2 proficiency test on the USGS NKT-1G iron basaltic glass microprobe standard by 64 laboratories are to be published by P. Potts et al.

except as noted in the composition results discussed below. Exceptions are elements present in low abundance: Ti, V, Ga, As and Se and occasionally Mn. Due to reduced total counts, the statistical error tends to be higher for low abundance elements in terminal particles. For higher abundance elements, measured mass uncertainty is dominated by the 7% uncertainty in the illuminated beam area estimated from measurements of the Fe thin film standard at different spot sizes (determined by vertical and horizontal scans of an absorbing edge through the focus spot). Error in Fe mass is dominated by uncertainty in the standard thickness and is at most a few percent.

IMPACT TRACK MAPPING AND ISOLATION OF COMETARY MATERIAL FROM BACKGROUND BY THRESHOLDING

Early optical microscopy on the Stardust impact tracks in aerogel during the preliminary examination (PE) period indicated that many of the comet dust particles were aggregates that broke apart into their constituents on impact. From a single entry hole in the aerogel, fine-grained particles were observed dispersed along some impact tracks, sometimes with multiple branches. Larger particles, denser, more mechanically robust and presumably comprised of larger grains, were located at the termini of these tracks. Subsequent studies (Hörz et al. 2006) have confirmed the aggregate nature of the dust. Due to the disaggregation of particles during hypervelocity capture, bulk composition measurements require measurement of material dispersed along entire impact tracks. As a result, we have collected full fluorescence spectra at each pixel in a map covering the impact track and surrounding aerogel for each keystone as did several of the synchrotron groups studying Stardust impact tracks. Even these whole-track maps may not fully include the total initial impactor mass since some vaporized and finely condensed material may be widely dispersed around the impact track and thus not entirely included in the width of the keystone and/or lost via sublimation from the entrance hole. By selecting energy windows about the fluorescence peak of a single element, for example, the Fe Kα peak, qualitative maps showing locations with high Fe abundance can be produced. Figure 2 shows such maps for Tracks 10 and 4 in the elements Fe, Ni, and Cr with warmer colors indicating greater fluorescence signal. In this manner, particles can be located by concentrated elemental abundances. The terminal end of Track 4, for example, contains two particles readily visible in the Fe map, each about 5 microns in diameter (FWHM in Fe signal) and separated by about 50 microns. Caution must be exercised, however, in generating simple energy-windowed element maps because of peak overlaps. For example, binning of signal in an energy window about the Mn Kα fluorescence peak at each map pixel will instead produce a map of the sum of the Mn Kα and Cr Kβ fluorescence plus contributions from the low-energy tail of the Fe Kα fluorescence.

Spectra from pixels containing cometary material may be summed to give a total spectrum from the entire impact track. Figure 3 shows an example of the total cometary material spectrum for Track 4. Note that the micro-SXRF spectra are plotted with fluorescence X-ray counts (intensity) on a logarithmic scale as a function of the emitted X-ray energy to allow the peaks associated with low abundance elements to be visible. Elements present in the cometary material spectrum include contributions from the aerogel subsequently removed via background subtraction. Spectra from pixels covering the terminal particle are then summed for a total spectrum from the terminal particle as well.

Silica aerogel has proven to be an excellent medium in many regards for the capture of particles at hypervelocity; however, it poses several challenges for SXRF analysis. Foremost is that Si and O are primary rock-forming elements, and their overwhelming contribution to the aerogel background makes quantification of Si and O impossible in the cometary material in aerogel keystones. The large amount of Si is also an absorber of Al and Mg fluorescence preventing meaningful quantification of these low-Z elements also important in silicate minerals. Two additional challenges affect the removal of the aerogel fluorescence background from spectra of cometary material in aerogel: First, the Stardust aerogel is density-graded with depth from about 5–50 mg/cm^3 to allow capture of both small and large particles. Second, there is significant contamination in the aerogel (Tsou et al. 2003) some of which has been observed to be non-uniformly distributed in aerogel tiles (Flynn et al. 2006, supporting online material). Figure 4 shows aerogel background spectra obtained away from the impact track in several of the aerogel keystones analyzed here. All of these keystones were extracted from a single aerogel tile, Cell 44. The variability of the contamination background with location is evident in the spectra. (Zn and Fe contamination as measured by ICP-MS (Tsou et al. 2003) are near 1.5–2.0 ppm by weight.) Zn is present in all the Stardust aerogel samples we have measured to date. This large background Zn contribution greatly reduces the sensitivity to Zn (increases the minimum detection limits) in the cometary material. Br is also present in large quantities in the aerogel but is not expected to be present in high abundance in average solar system materials. The Track 5 aerogel background spectra show anomalously high levels of Cr, Mn, Fe, Ni, Cu, and As, many elements typically associated with steels, as well as Pb. These spectra were collected several hundreds of microns below the original aerogel surface and away from the impact track itself. The cause of the high background levels seen in Track 5 is unclear. It could be highly non-uniform pre-existing contamination from aerogel tile manufacture or contamination during keystone preparation, handling, or storage after track extraction.

Accurate subtraction of the aerogel background is critical to precise comet dust composition measurements. The standard approach for background subtraction is to measure the

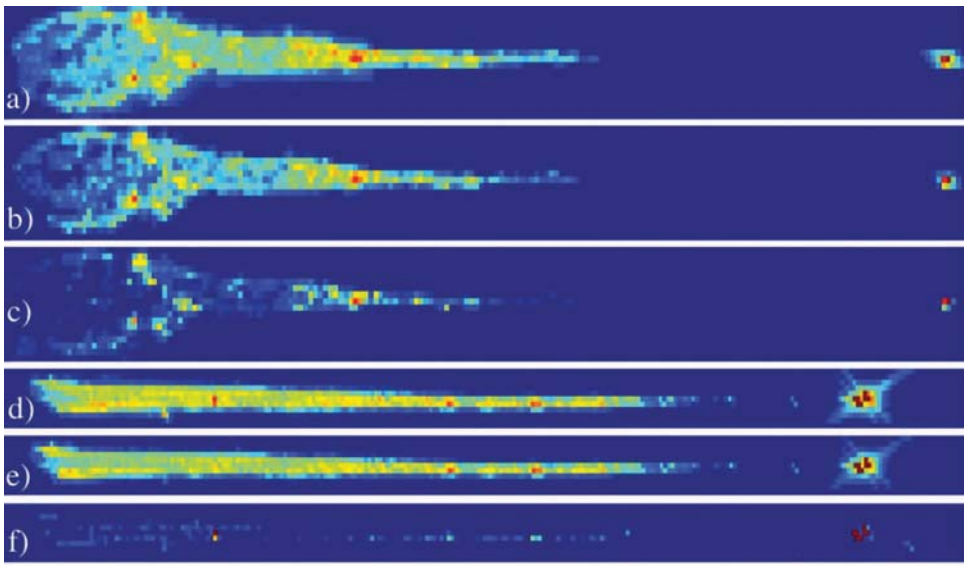

Fig. 2. X-ray fluorescence maps for two different shapes of Stardust impact tracks generated by setting energy windows encompassing relevant Kα lines. Maps of Track 10, an impact track with a bulbous shape, are shown in a) Fe, b) Ni, and c) Cr. Warmer colors indicate higher fluorescent intensity on a logarithmic scale. Track 10 is 2.8 mm from entrance hole to terminal particle. Analogous X-ray fluorescence maps are shown for Track 4, a carrot-shaped, conical impact track, in d) Fe, e) Ni, and f) Cr. Track 4 is 3.3 mm in length, and the terminal end of the Track 4 impact track contains two distinct ~3–4 micron diameter FWHM Fe-rich regions separated by ~50 microns.

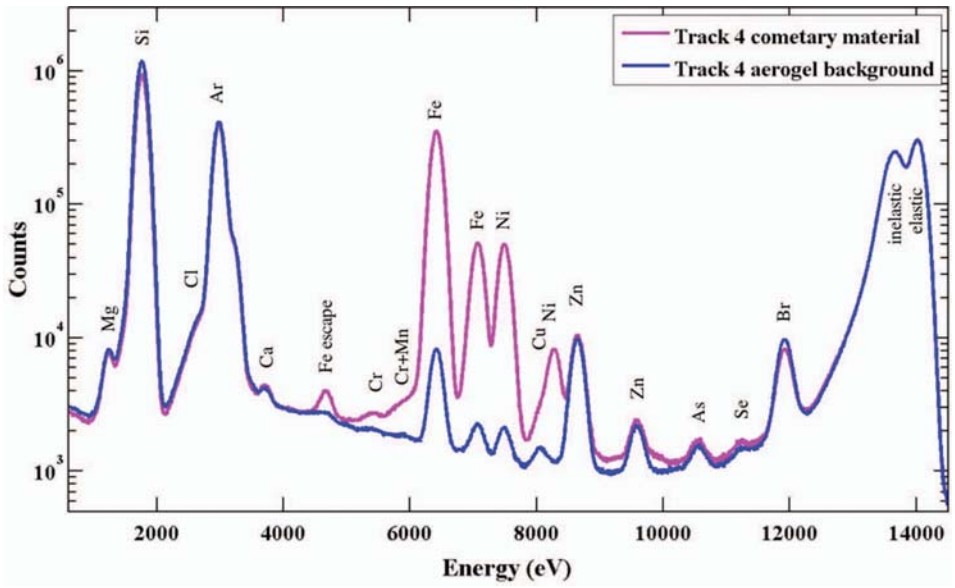

Fig. 3. X-ray fluorescence spectrum (magenta) plotted on a logarithmic scale from the cometary material in Stardust Track 4. Elements present in the cometary material spectrum include contributions from the aerogel (spectrum in blue, normalized) that is present above and below the cometary material in the X-ray beam path through the keystone.

background spectrum in a region containing no sample and subtract it from the total spectrum from the region of interest, in our case, the map of the comet dust impact track. One concern is the effectiveness of aerogel background removal for material embedded in melted and compacted aerogel in track walls. For measurement of compositions of complete impact tracks, we must make the assumption that the volume of aerogel, although melted and compacted in track walls, is conserved. We also assume that, locally, the contaminant distribution in the aerogel is uniform so that there is no loss or concentration of aerogel contaminants over the entire volume mapped. Terminal particles normally have compacted and melted aerogel associated with them, so pixels in isolated terminal particle maps may include more aerogel than pixels off the impact track. Compacted and/or melted aerogel will also contain higher levels of aerogel contaminant species per

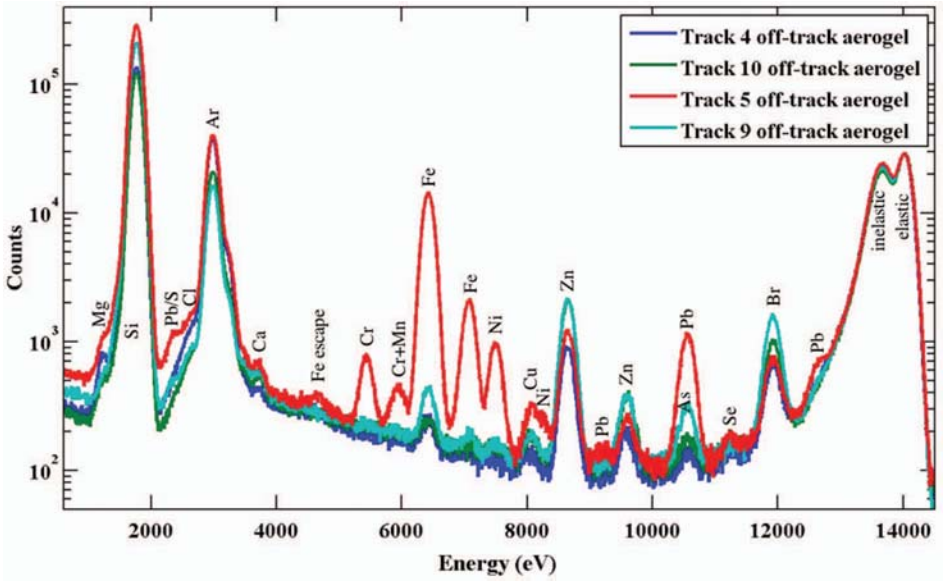

Fig. 4. Comparison of fluorescence spectra collected away from impact tracks in several of the Stardust aerogel keystones extracted from the Cell 44 aerogel tile. Ar is present due to excitation in air, and all keystones contain high Si, Zn, and Br contamination levels and, typically, some measurable Ca, Fe, Ni, Cu, As, and Se. There can be significant variation in aerogel background contamination at different locations within the same tile. The Track 4 keystone has relatively low contamination levels but exhibits more Mg than the others. The Track 5 keystone contains significant amounts of Pb in addition to much higher levels of Cr, Fe, Ni, and Cu than the other keystones. These high contamination levels are present in multiple locations on that keystone several hundreds of microns below the original aerogel surface and away from the impact track.

pixel. To account for these effects, we normalize the aerogel background spectrum to have equivalent elastically scattered signal to the cometary material spectrum rather than normalizing by the number of pixels. This is intended to minimize any apparent, but artificial, increase in the measured abundance of those elements that are present as contaminants in the aerogel and also as trace or minor elements in the cometary material.

Although aerogel background spectra can be obtained far from the comet dust impact track in nominally pristine aerogel and subtracted from the summed spectra in the impact track map, it is highly desirable to instead isolate those map pixels containing cometary material from those containing only aerogel. The near-track aerogel pixels may then be summed to generate a local aerogel background spectrum which can be subtracted from the summed cometary material spectrum. There are three primary advantages to this approach:

1. The aerogel has a non-uniform contaminant distribution so that a local aerogel sample is most accurate for background subtraction,
2. The aerogel has gradual variations in density due to manufacture and in thickness due to sample preparation, and
3. Inclusion of aerogel-only pixels in the total spectrum with cometary material pixels dilutes the total spectrum decreasing sensitivity to elements present in the cometary material.

The simplest implementation of this approach is to establish a single threshold level with which to divide map pixels into two categories: above the threshold, a pixel is considered cometary material, and below, it is considered aerogel. This "single threshold" approach has been used to analyze much of the Stardust impact track data previously presented in Flynn et al. (2006), including those that were measured at SSRL. Threshold levels based on the scatter peak area and the Fe fluorescence peak area have been explored and generally give nearly identical results. Synchrotron X-ray microprobes are highly sensitive to transition elements, and Fe is commonly found in the Stardust samples. Of all the quantifiable elements, Fe shows the strongest signal in all the tracks we measured. Based on our observations by transmission electron microscopy (TEM) (see also Zolensky et al. 2006), it is readily dispersed down impact tracks in the form of beads of Fe(Ni)-sulfides and -metal encased in aerogel and surrounding other cometary mineral components. Even around silicate terminal particles, these Fe-containing beads, typically nanometers to tens of nanometers in diameter, are present and closely associated with the silicate mineral grains. Given the relatively large pixel sizes used in these SXRF maps (approximately 10 to 15 microns) and high sensitivity to Fe, these silicate-dominated impact tracks are traceable by Fe. As such, the Fe signal is a reasonable choice for identification of cometary material, and the Fe fluorescence peak area has been used most frequently in our work. To account for expected variations in aerogel density

and keystone thickness, we have selected map locations in the aerogel and defined a threshold *surface*. This surface is adjustable by a scaling factor to fine-tune the boundary between the aerogel and the cometary material.

There is a significant risk associated with this "single threshold" technique, however: inadvertent inclusion of some cometary material in the background. Due in part to the relatively large map pixel sizes used for efficient data collection, there are border pixels on the edges of the two-dimensional map which can be considered to contain dirty aerogel contaminated by a bit of cometary material: They contain large amounts of aerogel as well as some cometary material. The map pixel sizes used are near the size of typical "large" particles seen in Stardust, on the order of 10 microns, so most, if not all, of this comet dust debris in a track is much smaller than the pixel size. (All of the map pixels in a keystone include some aerogel that contains no cometary material. In a pixel that includes a comet particle, for example, this aerogel lies above and below the particle in the keystone along the X-ray beam path.) As a result, there is no single threshold value that can neatly separate aerogel background from cometary material. If a sufficient number of these border pixels are included in the aerogel background, then significant amounts of cometary material may be included in the aerogel background spectrum. This inadvertent inclusion of some cometary material in the background results in subtracting it from the cometary material twice, first by not including it in the cometary material spectrum and again by subtracting it from the cometary material spectrum during background subtraction. The outcome is an underestimation of the abundances of elements in the cometary material. Inclusion of cometary material in the aerogel background category can be caused by a poorly set threshold or simply by cometary material that is not strongly associated with Fe. To address this risk, we have developed a "dual threshold" approach that we propose as a single analysis protocol to produce more precise average composition results from Stardust comet dust samples in the future.

The "dual threshold" approach involves establishing two thresholds, an upper threshold above which a pixel is considered to contain cometary material, and a lower threshold below which it is considered to contain only aerogel. Between the lower and upper thresholds is the third category: pixels to be discarded due to uncertainty. The spectra from pixels in the three categories are summed to generate total cometary material, discarded material and aerogel spectra. The primary advantage of this approach is the ability to observe and assess the material in the border pixels that contain mostly aerogel but, cumulatively, potentially significant amounts of cometary material as well. The lower threshold is set by decreasing it stepwise in steps corresponding to approximately 3–5% of the total range and observing the intensities of elements in the resulting aerogel background sum spectra. Below a certain lower threshold level, the area of the Fe peak relative to the Si peak stops decreasing in the aerogel background sum spectrum, and this lower threshold level is selected. (The Fe/Si peak area ratio can be plotted with decreasing lower threshold level to determine the lower threshold level at which the ratio stabilizes to the aerogel background level.) The local aerogel background spectrum obtained is compared with spectra collected away from the impact track to make sure it is similar. It is generally not identical due to variations in aerogel composition in the aerogel tile. The upper threshold is then set in a similar manner by watching the discarded sum spectrum. The ideal upper threshold is chosen where the discarded sum spectrum has similar relative intensities for those elements present in the cometary spectrum but not present in the aerogel spectrum, and the total Fe mass in the discarded sum spectrum is small relative to the cometary material sum spectrum. Ideally, the discarded sum spectrum equals a fraction of the cometary sum spectrum, and this ensures that the discarded pixels contain the same average composition as the cometary pixels and will not significantly impact the total composition results. If the upper threshold value is lowered until the total Fe mass in the discarded sum spectrum is less than 1% of the total cometary Fe, and the discarded sum spectrum does not have similar relative intensities for those elements present in the cometary spectrum, that is, it does not show the same average composition, then closer inspection is warranted to determine if material not associated with Fe is present. The following section gives two examples of such cases, one an aerogel contaminant in the discarded sum spectrum and the other non-Fe-associated cometary material subsequently included in the cometary spectrum. In Track 10, the only track without aerogel contaminants or non-Fe-associated cometary material, adding the discarded material and cometary material spectra together give increases in the cometary material of less than 1% in Fe, Ni, and Cu mass abundances, 2–4% for Mn, Zn, and Ca and 14% for Se which is present near its detection limit. It should be noted that the discarded pixels, a small fraction of the projected two-dimensional map area containing cometary material, are an even smaller fraction of the three-dimensional volume in the keystone containing cometary material. In this manner, conservative lower thresholds can be established to ensure aerogel backgrounds clean of cometary material, and upper thresholds can be set to minimize inclusion of background aerogel while making certain that large amounts of cometary material are not discarded.

Figure 5a contains the resulting total sum spectra (on a log scale) for cometary material (magenta), normalized aerogel background (blue), and discarded material (black) for Track 4. The aerogel background is scaled to have the same intensity in the elastically scattered X-ray peak at 14 keV. The discarded material spectrum is displayed on the same scale as the cometary material spectrum to illustrate the relatively small amount of material discarded. Note that

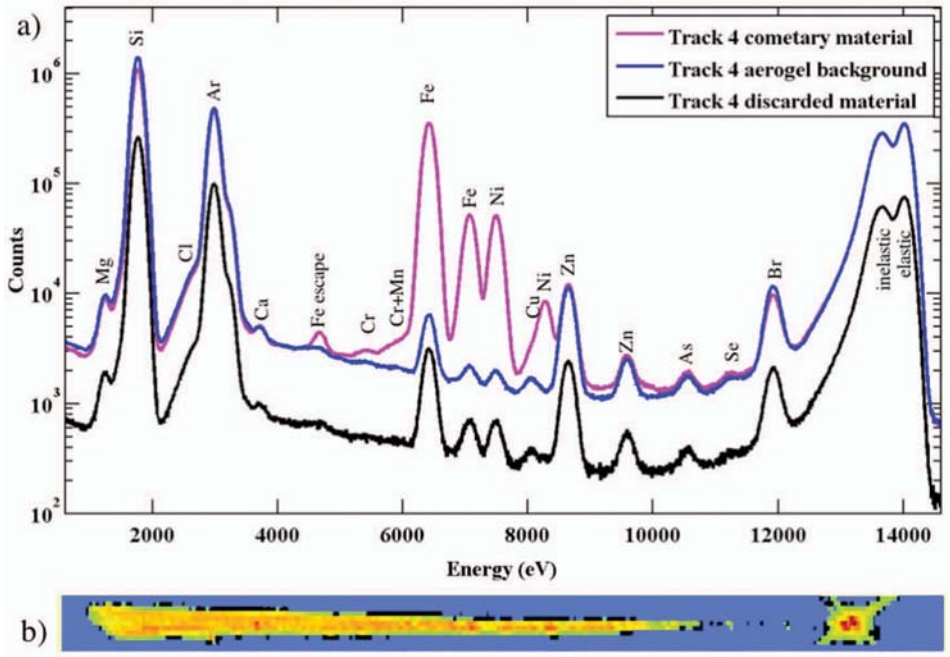

Fig. 5. Results of dual threshold analysis of Stardust Track 4. a) Sum spectra generated by the dual threshold approach for cometary material (magenta), normalized aerogel background (blue), and discarded material (black) for Track 4 in its entirety. b) Fe signal in the map of Track 4 after applying dual thresholds: pixels in the light blue region are designated aerogel, pixels in the black region are discarded, and pixels in the multi-colored yellow through red region are designated cometary material. The spectra in these three categories of pixels were summed to produce the fluorescence spectra in a).

Table 2. Element abundances by mass for Stardust impact Track 12 by single and dual threshold analysis.[a]

	Single threshold mass (g)	Dual threshold mass (g)	Ratio (dual/single)
Cl	3.05E-11	5.78E-11	1.89
K	6.19E-12	1.27E-11	2.04
Ca	2.07E-13		
Cr	5.92E-12	8.51E-12	1.44
Mn	4.37E-14	6.17E-14	1.41
Fe	2.89E-10	2.98E-10	1.03
Ni	2.48E-11	2.58E-11	1.04
Cu	1.52E-13	3.10E-13	2.04
Zn	2.15E-13	8.83E-13	4.11
Ga	2.12E-14		
As	1.39E-13	2.48E-13	1.78
Se	2.09E-13	2.05E-13	0.98
Total	3.57E-10	4.04E-10	1.13

[a]Measured masses above minimum detection limits are reported here.

the amplitudes of peaks in the discarded material spectrum are about 100× smaller than those in the cometary material spectrum for the elements Fe and Ni. Figure 5b shows the Fe signal in the dual thresholded map. The light blue region contains those pixels categorized as containing only aerogel, the black region contains those pixels discarded, and the yellow through red region contains those pixels categorized as containing cometary material with red indicating the highest fluorescent intensities. The shape and size of the cometary material region matches the optically visible impact track. As one would expect, the discarded pixels lie at the outline of the impact track—the so-called border pixels discussed above. The discarded pixels do not include pixels located within the surrounding aerogel-only region, so any inherent aerogel contamination "hot spots" (Flynn et al. 2006, supporting online material) are included in the resulting aerogel background spectrum. (This might not be the case were we to generate the X-ray maps with finer spatial resolution.)

To illustrate the potential impact of dual threshold versus a single threshold analysis, Table 2 contains the element mass abundances for Stardust impact Track 12 obtained using each approach and the fractional change in mass abundance in changing from single threshold analysis to dual threshold analysis. The changes in this case are due primarily to a more conservative lower threshold established by the procedures given above and the inclusion of Cr not strongly associated with Fe (discussed below). Calcium and Ga, elements previously measurable above background using the single threshold analysis, are no longer measurable by dual threshold analysis due to changes in minimum detection limits. Thirteen percent more total mass is found to be cometary using the dual threshold analysis due to cometary material no longer being incorrectly added into the aerogel background spectrum. The most abundant elements, i.e., Fe and Ni, are not significantly impacted since Fe is used to establish the threshold level(s) in both the single and dual threshold analyses. The Cr and Mn

abundances increase by about 40%. The trace elements, Cu, As and K, increase 2-fold, and the Zn abundance increases 4-fold. As a rule, slight variations in threshold levels have a larger impact on trace and minor element abundances than on major element abundances using either single or dual threshold analysis. Trace element abundances are especially sensitive to the exact details of the analysis. This is a strong motivation for an established analysis approach uniformly applied to Stardust track composition analysis.

The possibility that the upper threshold might exclude some cometary particles of atypical composition is a concern that is addressed to some extent by close examination of the discarded material sum spectrum (next section). We mention here another potential approach for analysis that involves generating thresholds based on each of the elements present in the impact track and cross-correlating multiple elements. The formal method of principle component analysis (PCA) can be quite effective in extracting the most significant clusters of components in certain classes of data sets. PCA would be ideal for extracting mineral phases in most analyses of mixed mineral assemblages; however, the case of Stardust impact tracks is strongly hampered by the inability to measure Si and O, major elements in many relevant minerals, above the aerogel background.

Four of the five Stardust tracks were analyzed with dual threshold analysis. The fifth, Track 5, was not mapped with sufficient surrounding aerogel to produce a reliable aerogel background. Since this keystone is small such that all of the aerogel is near the track, several off-track aerogel spectra were summed and used as the background spectrum. In practice, typically less than 1% of the total Fe mass is discarded from an impact track. In Track 9, about 1.5% of the Fe mass was discarded due to the presence of localized contamination discussed below. The impact track and terminal particle composition results are discussed below in more detail.

DUAL THRESHOLD ANALYSIS AS A DIAGNOSTIC TOOL

The "dual threshold" approach allows a close examination of the summed spectra in the discard category. This is important for locating high concentrations of elements that are *not* strongly associated with Fe. As one example, close examination of Track 12 showed that there were map pixels with significant Cr *not* strongly associated with Fe, and these pixels were mistakenly placed in the discard category in the early analyses. By lowering the upper threshold to include more pixels with lower Fe intensities, the Cr-containing pixels were included in the cometary material. Because measurements in silica aerogel are effectively blind to Si, and there are a lot of silicates in the Stardust sample, we are including and measuring those silicates primarily based on other heavier elements present such as Fe, Cr, and Mn. Including pixels with minor elements, potentially underrepresented by other analysis methods that rely on the Fe fluorescence signal, helps to ensure analysis of the majority of the cometary material. These minor elements are critical for eventually obtaining a valid measurement of the Wild 2 average composition.

Another example of "dual threshold" analysis as a diagnostic tool illustrates a discovery also of significance for other Stardust impact track studies. Early analysis of a few of the impact tracks we studied showed the presence of a significant amount of gold. This was a very unexpected and suspicious result, because the average solar abundance (assumed to be representative of the material from which all solar system objects formed) (Lodders 2003) for the element gold is 2–3 orders of magnitude below the experimental minimum detection limits for the samples and data collection parameters used in this work. In Track 5, the Au level was measured to be 5 orders of magnitude greater than solar abundance. Mapping of the Au Lβ line in this track is difficult due to peak overlaps with Zn and Br, and the Au appears to be mixed with cometary material in the track at the size scale of the X-ray beam spot. After bemused speculation regarding future Au mining on comets, dual threshold analysis of another track revealed the Au to be a contaminant rather than indigenous to the cometary material. The discard spectrum of Track 9 revealed the presence of additional Au contamination without significant Fe present. Mapping of the Au signal showed it to be localized at the aerogel surface, possibly flakes from an autoclave used in aerogel processing. Figure 6 contains the Fe Kα and Au Lβ fluorescence maps. The Au contamination location is offset from the impact track entrance hole and thus not associated with the original cometary particle. When the Fe signal alone is used to set the threshold for cometary material, several pixels including Au from this surface contamination are included in the cometary material. Figure 7a shows the whole impact track cometary material and aerogel background spectra resulting from applying dual thresholds first based on Fe fluorescence and then an additional single threshold based on Au fluorescence to remove contaminated pixels. Figure 7b shows the spectrum of the pixels containing with high Au fluorescence unambiguously identified by both the Lα and Lβ lines. Together these pixels contain about 0.45 nanograms of Au which, if included in the cometary material for all five tracks measured in this work would have been about 150,000 times solar abundance levels. Other elements present most likely arise from some cometary material present in the pixels containing Au; however, it is not possible to say for certain at this time if the contamination is pure elemental Au. The Au contamination may be present only in the batch of aerogel cells to which Cell 44 belongs, or it may be more widespread. Because Au was found well-separated from Track 9, it is most probable that the Au intermixed with cometary material in other tracks is also due to surface contamination that has been entrained during the hypervelocity capture process and carried down the track with cometary particles.

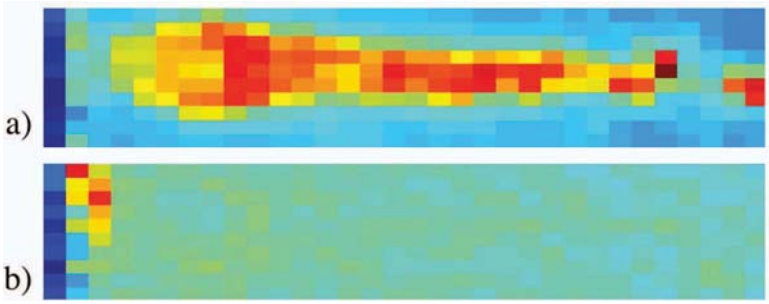

Fig. 6. X-ray fluorescence maps for Track 9 generated by setting energy windows encompassing a) the Fe Kα and b) the Au Lβ lines. Au contamination is located at the aerogel surface and is clearly not associated with the comet dust impact track.

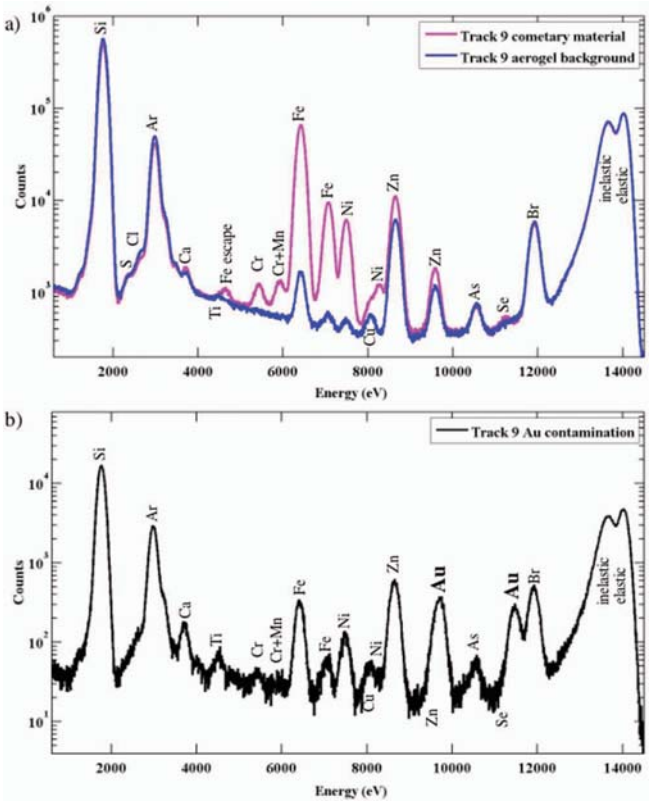

Fig. 7. Results of dual threshold isolation of cometary material for Track 9. a) Sum spectra for cometary material and normalized aerogel background for Track 9 in its entirety, and b) the sum spectrum of those pixels containing Au fluorescence isolated from the map of Track 9.

COMPOSITION RESULTS AND DISCUSSION

Cometary material containing approximately 3.8 nanograms of Fe is found in the five Stardust impact tracks analyzed in this work. (Should solar system abundances prove appropriate for this portion of the Stardust sample, the approximate total mass analyzed is >20 nanograms.) In many tracks, the total mass deposited along an impact track is dominated by the terminal particle; however, in others, a significant fraction of the cometary material is fine-grained and distributed along the length of the impact track embedded in the aerogel glass forming the track walls. In sulfide-dominated particles (and sub-particles), fine beads of Fe(Ni)-sulfides and Fe(Ni) metal/oxide are found deposited along the entire track. This is evident in other tracks studied by optical microscopy followed by particle extraction and electron microscopy, and although we present a very limited sample set, we see similar results in our micro-SXRF mass measurements. Table 1 shows that carrot-shaped, conical tracks tend to have large percentages of their Fe mass located in the terminal particle while tracks with more bulb-like shapes near the impact surface tend to have lower percentages of Fe mass in the terminal particle. All of the terminal particles of the 5 Stardust tracks measured were less than 5 microns in diameter as measured by Fe fluorescence signal. It is important to note that due to the combined effects of large

amounts of Si in the aerogel and measurements carried out with some Ar from air in the beam path to the detector, the micro-SXRF mass measurements are effectively blind to Fo-rich olivine and En-rich, low-Ca pyroxene, both dominated by Mg, Si, and O. Particles dominated by these minerals have been found frequently in Stardust samples (Zolensky et al. 2006). It is common, however, that these particles have glass with beads of Fe(Ni)-sulfide and Fe(Ni)-metal adhered on them, so the micro-SXRF technique can locate such a terminal particle, but it may underestimate the true particle size and will certainly underestimate the true particle mass since Si, O, Mg, Al, C, and H are not quantifiable with any certainty and are not reported here.

The compositions of each of the 5 Stardust impact tracks and their terminal particles are given in Table 3 in mass and in Table 4 in moles. (Whole impact tracks include the terminal particle.) For elements not detected, the detection limit (specific to each element in each sample and the data collection parameters) is listed in italics. Si, O, Mg, Al, C and H are not quantified due to the aerogel background and absorption. The high levels of Br present in the aerogel and Ar due to air scatter are also not quantified in this work. Levels of Pb low enough that the Pb Lβ line is not strongly excited are indistinguishable from low levels of As under the experimental conditions for these measurements. Since Pb is present in the Track 5 aerogel background, it is possible that As abundances are overestimated in these tables due to the presence of contaminant Pb. Note that minimum detection limits are affected by surrounding element abundances as well as X-ray count time per pixel and thus are not fixed for a given element. Minimum and maximum mean abundances for the impact tracks and terminal particles in Table 4 were calculated by taking the abundances of elements not detected (non-detects) as zero and as the minimum detection limit, respectively.

In seeking to narrow the uncertainties in bulk composition measurements of the Wild 2 comet dust, improved accuracy in composition measurements is highly relevant. Due to the very limited number of Stardust tracks analyzed thus far since the sample return, there are large uncertainties associated with the Wild 2 element abundances currently available in the study by (Flynn et al. 2006). Replacing the initial composition results for these five Stardust tracks in the above study with the refined dual threshold values reported here in Tables 3 and 4 results in a shift of up to 9% in the average abundances of some elements reported in (Flynn et al. 2006). These five tracks comprise only 20% of the tracks included in that study. The shifts in average abundance fall within the current uncertainty levels; however, with greater number of analyses added in the future, such shifts will become significant. The data in Table 4 can be combined with additional composition measurements in the future to develop more robust statistical mean elemental abundances for the Stardust comet sample than are currently available. Such data will allow closer comparisons with other classes of extraterrestrial materials typically via normalization by Fe and the solar abundance (Lodders 2003). (The current sample size of five keystones is insufficient to provide a meaningful average composition and thus normalization by solar abundance is not useful.)

Interestingly, Zn is measured in most of the impact tracks but in none of the terminal particles even though the detection limits are generally 2 to 3 orders of magnitude lower for terminal particles. Since there is a lot of background Zn in the aerogel, this raises the question of whether contaminant Zn might be concentrated in the impact track walls. Sulfur from the cometary material is a possible getter for Zn, and a close look at Zn-containing sulfides is warranted. Other mobile contaminants in the aerogel such as Sn, which has also been observed in some sulfides in TEM studies of other samples, may be subject to gettering in the same manner. Another possibility is that most of the Zn from impacting comet dust particles is volatilized during impact and lost to the surrounding aerogel. This process would have to be efficient to explain the non-detection of Zn in the terminal particles in tracks that show Zn abundances. If this is the case, then it is likely that not all Zn originally present in the cometary material has been included in these measurements. It is also noteworthy that, even for grain sizes of a few microns, the S abundance in Fe-sulfides is almost certainly underestimated in this work due to incomplete correction of absorption effects from Fe (and/or Ni) and S volatilization during impact. However, the S/Fe ratio may also be expected to be lower than in the original impacting particle due to sublimation on impact and during the spacecraft's return trip.

Each of the 5 Stardust tracks and their terminal particles is discussed in more detail below. Table 5 contains the abundances (in moles) of the measured elements normalized by Fe for each impact track and terminal particle. (Solar abundances (Lodders 2003) similarly normalized are also given for completeness; however, such comparisons are best made with the average composition of many particles.) The element/Fe stoichiometric ratios are only given for quantified elements for simplicity and to facilitate discussion of each track and terminal particle. In some cases, it is straightforward to recognize the dominant mineralogy in a terminal particle while in others, the inability to quantify Si, a major rock-forming element, combined with a likely cocktail of minerals makes even educated guesswork impossible. From TEM results (Zolensky et al. 2006), it is known that the Stardust sample includes large single-mineral grains of sulfides and silicates and more exotic minerals as well as aggregates of many mineral phases, more fine-grained crystal grains with coatings of glass containing beads of Fe(Ni)-sulfides and Fe(Ni)-metal. Large single mineral grains are frequently not isolated but have neighboring smaller grains of other, different mineral phases and glassy material containing sulfide alteration products. In general, Zn and Se tend to reside in the Fe-sulfides, and high Ni content in the sulfides has

Table 3. Abundances of measured elements in Stardust comet particle impact tracks and terminal particles by mass.[a]

Mass (g)	S[b]	Cl	K	Ca	Ti	V	Cr	Mn	Fe	Ni	Cu	Zn	Ga	Ge	As[b]	Se	Total
Track 4 (C2044,0,38)	*4E-12*	*4E-12*	2.5E-11	6.7E-12	*3E-13*	*2E-13*	*1E-13*	*1E-13*	1.2E-09	1.1E-10	9.0E-13	*9E-14*	*3E-14*	2E-13	*3E-14*	*3E-14*	1.4E-09
terminal particle	*1E-12*	*1E-12*	4E-12	1E-12	4E-13	*6E-14*	*5E-14*	2E-13	4.0E-10	3.1E-11	3.2E-13	*3E-14*	2E-14	7E-14	*1E-14*	*1E-14*	4.4E-10
Track 5 (C2044,0,39)	2.2E-11	*2E-13*	*1E-13*	2.2E-12	2.7E-13	9E-14	4.8E-12	4.6E-13	1.2E-11	1.7E-12	4.3E-13	2.4E-13	*2E-15*	*1E-15*	*4E-15*	*1E-15*	4.6E-11
terminal particle	*3E-14*	*3E-14*	*1E-14*	1.4E-13	1E-14	*1E-15*	1.4E-13	1.7E-13	2.5E-13	9.2E-15	2E-15	*6E-16*	*2E-16*	*2E-16*	*5E-16*	*2E-16*	7.2E-13
Track 9 (C2044,0,42)	9E-12	*8E-13*	*4E-13*	2E-12	*7E-14*	*5E-14*	1.3E-12	7.8E-13	1.1E-10	6.4E-12	*1.2E-14*	4.3E-12	*8E-15*	*8E-15*	*9E-15*	4E-14	1.4E-10
terminal particle	2E-12	*2E-13*	*8E-14*	7E-14	*2E-14*	*1E-14*	4E-14	*6E-15*	6.9E-12	8.5E-13	*3E-15*	*7E-15*	*2E-15*	*2E-15*	*2E-15*	3E-15	9.9E-12
Track 10 (C2044,0,43)	*6E-12*	*5E-12*	*2E-12*	4.8E-11	2E-12	*3E-13*	2.2E-11	9.8E-12	2.1E-09	9.7E-11	7.7E-12	1.9E-11	*4E-14*	*3E-14*	*4E-14*	3E-13	2.4E-09
terminal particle	6E-12	3E-12	*3E-13*	7E-13	*5E-14*	*4E-14*	1.1E-12	9.8E-13	2.0E-10	5.8E-12	1E-13	*2E-14*	*5E-15*	*5E-15*	*5E-15*	2E-14	2.2E-10
Track 12 (C2044,0,52)	*5E-12*	5.8E-11	1.3E-11	*4E-13*	*1E-13*	*1E-13*	8.5E-12	6E-14	3.0E-10	2.6E-11	3.1E-13	8.8E-13	*2E-14*	*2E-14*	2.5E-13	2.1E-13	4.0E-10
terminal particle	*1E-12*	*6E-13*	*2E-13*	1E-13	*4E-14*	*3E-14*	8.5E-13	1.5E-13	8.9E-11	6.1E-12	*5.6E-15*	*1.2E-14*	*4E-15*	*4E-15*	2E-14	*4E-15*	9.7E-11

[a]Impact tracks include the terminal particle. For non-detects, the detection limit is given in italics for each element and each measurement. The measured Mn abundance in Track 12 is at the detection limit.
[b]See text for discussion of As in general and S in Track 5.

Table 4. Abundances of measured elements in Stardust comet particle impact tracks and terminal particles by atoms (moles).[a]

Atoms (moles)	S[b]	Cl	K	Ca	Ti	V	Cr	Mn	Fe	Ni	Cu	Zn	Ga	Ge	As[b]	Se	Total
Track 4 (C2044,0,38)	*1E-13*	*1E-13*	6.5E-13	1.7E-13	*6E-15*	*4E-15*	*3E-15*	*2E-15*	2.2E-11	1.9E-12	1.4E-14	*1E-15*	*4E-16*	3E-15	*4E-16*	*3E-16*	2.5E-11
terminal particle	*4E-14*	*4E-14*	1E-13	3E-14	9E-15	*1E-15*	*9E-16*	*3E-15*	7.2E-12	5.3E-13	5.0E-15	*5E-16*	3E-16	1E-15	*1E-16*	*1E-16*	7.9E-12
Track 5 (C2044,0,39)	6.9E-13	*6E-15*	*3E-15*	5.5E-14	5.7E-15	2E-15	9.3E-14	8.4E-15	2.2E-13	2.9E-14	6.7E-15	3.6E-15	*2E-17*	*2E-17*	*5E-17*	*2E-17*	1.1E-12
terminal particle	*1E-15*	*7E-16*	*3E-16*	3.4E-15	2E-16	*2E-17*	2.7E-15	3.1E-15	4.5E-15	1.6E-16	3E-17	*9E-18*	*3E-18*	*2E-18*	*6E-18*	*2E-18*	1.4E-14
Track 9 (C2044,0,42)	3E-13	*2E-14*	*1E-14*	4E-14	*2E-15*	*1E-15*	2.4E-14	1.4E-14	2.0E-12	1.1E-13	*1.9E-16*	6.6E-14	*1E-16*	*1E-16*	*1E-16*	5E-16	2.5E-12
terminal particle	6E-14	*5E-15*	*2E-15*	2E-15	*3E-16*	*2E-16*	8E-16	*1E-16*	1.2E-13	1.4E-14	*4E-17*	*1E-16*	*3E-17*	*2E-17*	*3E-17*	4E-17	2.1E-13
Track 10 (C2044,0,43)	*2E-13*	*1E-13*	*6E-14*	1.2E-12	4E-14	*5E-15*	4.1E-13	1.8E-13	3.8E-11	1.7E-12	1.2E-13	2.8E-13	*5E-16*	*5E-16*	*5E-16*	4E-15	4.2E-11
terminal particle	2E-13	9E-14	*8E-15*	2E-14	*1E-15*	*7E-16*	2.1E-14	1.8E-14	3.6E-12	9.8E-14	2E-15	*3E-16*	*8E-17*	*6E-17*	*7E-17*	2E-16	4.0E-12
Track 12 (C2044,0,52)	*1.5E-13*	1.6E-12	3.2E-13	*9E-15*	*3E-15*	*2E-15*	1.6E-13	1E-15	5.3E-12	4.4E-13	4.9E-15	1.4E-14	*2E-16*	*2E-16*	3.3E-15	2.6E-15	7.9E-12
terminal particle	*3.7E-14*	*1.6E-14*	*4.7E-15*	3E-15	*7.3E-16*	*4.6E-16*	1.6E-14	2.7E-15	1.6E-12	1.0E-13	*8.8E-17*	*1.8E-16*	*5E-17*	*5E-17*	2E-16	*5E-17*	1.7E-12
Min mean (tracks)	9.7E-13	1.6E-12	9.7E-13	1.5E-12	4.4E-14	1.7E-15	7.0E-13	2.0E-13	6.8E-11	4.2E-12	1.5E-13	3.7E-13	0.0E+00	2.7E-15	3.3E-15	6.7E-15	7.9E-11
Min mean (particles)	2.6E-13	9.0E-14	1.0E-13	1.2E-12	9.3E-15	0.0E+00	4.1E-14	2.6E-14	1.3E-11	7.5E-13	7.0E-15	0.0E+00	2.8E-16	1.0E-15	2.0E-16	2.6E-16	1.4E-11
Max mean (tracks)	1.4E-12	1.9E-12	1.0E-12	1.5E-12	5.4E-14	1.3E-14	7.0E-13	2.0E-13	6.8E-11	4.2E-12	1.5E-13	3.7E-13	1.3E-15	3.4E-15	4.3E-15	7.1E-15	7.9E-11
Max mean (particles)	3.4E-13	1.5E-13	1.2E-13	1.2E-12	1.1E-14	2.6E-15	4.2E-14	2.6E-14	1.3E-11	7.5E-13	7.2E-15	1.1E-15	4.3E-16	1.1E-15	4.3E-16	4.2E-16	1.4E-11

[a]For non-detects, the detection limit is given in italics for each element and each measurement. The minimum and maximum mean values for elemental abundances in the whole impact tracks and terminal particles are given at the bottom of the table. The minimum mean is calculated by setting the abundance of all non-detected elements to zero, and the maximum mean is calculated by setting the abundance of non-detected elements to the minimum detection limit for that element.
[b]See text for discussion of As in general and S in Track 5.

Table 5. Abundances (moles) of measured elements normalized by Fe in Stardust comet particle impact tracks and terminal particles.[a]

Element/Fe	S[b]	Cl	K	Ca	Ti	V	Cr	Mn	Fe	Ni	Cu	Zn	Ga	Ge	As[b]	Se
Solar abundances[c]	5.31 E-01	6.25 E-03	4.41 E-03	7.50 E-02	2.89 E-03	3.44 E-04	1.54 E-02	1.09 E-02	1.00E+00	5.70 E-02	6.29 E-04	1.46 E-03	4.29 E-05	1.44 E-04	7.27 E-06	7.85 E-05
Track 4			3.0E-02	7.6E-03					1.0E+00	8.8E-02	6.4E-04			1E-04		
terminal particle			1E-02	4E-03	1E-03			4E-04	1.0E+00	7.4E-02	7.0E-04		4E-05	1E-04		
Track 5	3.2E+00			2.5E-01	2.6E-02	8E-03	4.3E-01	3.8E-02	1.0E+00	1.3E-01	3.1E-02	1.7E-02				
terminal particle				7.7E-01	5E-02		6.1E-01	6.8E-01	1.0E+00	3.5E-02	7E-03					
Track 9	1E-01			2E-02			1.2E-02	7.0E-03	1.0E+00	5.4E-02		3.3E-02				3E-04
terminal particle	5E-01			1E-02			6E-03		1.0E+00	1.2E-01						3E-04
Track 10				3.1E-02	1E-03		1.1E-02	4.6E-03	1.0E+00	4.3E-02	3.2E-03	7.4E-03				9E-05
terminal particle	5E-02	3E-02		5E-03			6.0E-03	5.0E-03	1.0E+00	2.8E-02	6E-04					6E-05
Track 12		3.1E-01	6.1E-02				3.1E-02	2E-04	1.0E+00	8.2E-02	9.1E-04	2.5E-03			6.2E-04	4.9E-04
terminal particle				2E-03			1.0E-02	1.7E-03	1.0E+00	6.5E-02					1E-04	

[a]Only measured elements above the minimum detection limits are shown in this table for simplicity.

[b]See text for discussion of As in general and S in Track 5.

[c]Solar abundance values (Lodders 2003) have been included for completeness; however, it is important to note that individual comet dust particles are not expected to have solar abundances, especially since many have been found to be dominated by large single mineral grains. Comparisons against solar values are best made with averages of many particles.

also been reported widely, probably a result of heating and preferential Fe loss over Ni. As the sulfides melt at lower temperatures than the silicates, tiny beads of sulfides are found distributed along tracks and around other particles in many Stardust impacts. Because we are blind to Si and O, it is not possible to distinguish with certainty between silicates and spinels; however, silicates are known from TEM studies to be present in much greater quantities in the Stardust sample. High Cr and Mn have been reported in Stardust silicates, so a particle with low Fe levels for its size (measured based on the Fe signal) and containing Cr and Mn might be dominated by silicate(s).

Track 12

Track 12 is a narrow, carrot-shaped track 1.6 mm in length with significant mass in the terminal particle. As the only track studied at multiple synchrotron X-ray microprobes during the PE period, Track 12 received extra scrutiny (Flynn et al. 2006, supporting online material). The total mass measured (dominated by Fe) is equivalent between the dual threshold results in Table 2 obtained at SSRL and the results reported from the National Synchrotron Light Source (NSLS). The Mn abundance in Track 12 is at the minimum detection limit, and the statistical error is 70%. For the terminal particle, the statistical error is 15% for As and 25% for Ca. (Other statistical errors are ≤10% by mass unless stated otherwise.) Based on the lack of measured S in Track 12 or its terminal particle and the presence of Cr and some Mn and Ca, it is likely that the Track 12 terminal particle is predominantly silicate material, olivine and pyroxene.

Track 10

Track 10 is 2.8 mm in length and is shown mapped in several elements in Figs. 2a–c. It has a bulb-shaped entrance with hot-spots of cometary material deposited in the bulb. The whole track Ti abundance has 15% statistical uncertainty, and the terminal particle Se abundance, 20% uncertainty. While S is below detection limits in the track, the terminal particle contains a S:Fe ratio of about 0.05:1. There is also significant Al (not quantified) above the background in the terminal particle. These suggest the presence of a mixture of mineral phases including some likely fine-grained metal-sulfide residues.

Track 9

Track 9 is a short, bulb-shaped track 0.5 mm in length. Isolation of the Au fluorescence signal in Track 9 led to the conclusion that Au is not indigenous to the Stardust comet dust but, instead, a near-surface contaminant in the aerogel collector tile. Pixels in the Track 9 map that contained approximately 0.45 nanograms of Au are excluded from the cometary material spectrum. In the terminal particle, the Se abundance has a statistical uncertainty of 20%; Ca, 23%; and Mn, 70%. Based on the relatively high S/Fe ratio, the terminal particle of Track 9 is likely dominated by Fe-Ni-sulfide. There is measurable S in the impact track also, but differing Ca/Fe, Cr/Fe and Mn/Fe levels between track and terminal particle indicate the probable presence of silicates in the track as well as sulfides.

Track 5

Track 5 is also a short, bulb-shaped track 0.3 mm in length. Since Au is clearly associated with the aerogel surface in Track 9, we assume that when it is present in other impact track maps from the same Cell 44 aerogel tile is not indigenous to the comet particles. In Track 5, Au contamination appears to have been struck by the impacting particle and dispersed down the impact track. Since it is intimately associated with the cometary material, we made no attempt to separate it out by identifying pixels containing Au. Au found in Track 5 is therefore believed to be due to entrainment of Au surface contamination in the aerogel rather than from the comet. As such, it is not reported in Tables 3, 4, and 5. A total of about 1.0 nanogram of Au was measured in the Track 5 impact track. There is no detectable Au associated with the terminal particle alone where the minimum detection limit was at the 0.4 femtogram level. It is assumed that the Au contamination was fully removed from the terminal particle during its transport down the track.

Insufficient surrounding aerogel was mapped around Track 5 to permit aerogel background isolation. As a result, we did not apply any thresholds on this track, and we used the aerogel background collected away from the track in the same keystone. This is a small keystone (<1 mm in length), and these background spectra were collected approximately 200–300 microns away from the optically visible track boundary in several different locations. It should be noted, however, that the aerogel background in this keystone contains anomalously high levels of Cr, Mn, Fe, Ni, Cu, and As, many elements typically associated with steels. Pb is also present in the Track 5 aerogel background and is removed from the whole track and terminal particle cometary material spectra by background subtraction. The high S stoichiometry in this track (see Table 5), more than two times greater than the sum of the Fe, Ni, and Zn present, indicates that the S Kα peak is likely contaminated with Pb Mα fluorescence that was not completely removed by background subtraction. As such, the S abundance in this track should be considered especially suspect. The statistical uncertainty in V in the track is 15%. The high levels of contaminants in the aerogel prevent determination of minerals present.

Track 4

Track 4 is a carrot-shaped track 3.3 mm in length and is shown mapped in several elements in Figs. 2d–f. The terminal

particle spectra from mapping this track were replaced with spectra taken with smaller spot size to reduce the impact of incomplete charge collection (which is detrimental to the signal-to-noise ratio and, therefore, elemental sensitivities). The Ti abundance in the terminal particle has a statistical uncertainty of 15%; Mn, 20%; and Ga, 30%. Mg and Al are well above aerogel background levels in the terminal particle, and Mg is above background in the whole track. S is below detectable levels for this track, and the presence of Ca and Mn indicate silicates are likely the principle component in this track. There is a total of about 0.14 nanograms of Au present in the terminal particle (or immediately adjacent to it), but the whole track analysis is not sensitive to the level of Au present. Au levels are low enough in this terminal particle that they can be obscured by neighboring peaks preventing isolation of Au via thresholds. This is unlike the situation with Track 9 where the Au Lβ line was strong enough to isolate by thresholding. (With future application of principle component analysis, we may be better able to isolate known contaminants from impact tracks.) As in Track 5 above, the Au is believed to due to entrainment of aerogel surface contamination and is not reported in the tables.

CONCLUSIONS

We have mapped five Stardust impact tracks in aerogel by micro-SXRF at the Stanford Synchrotron Radiation Laboratory collecting full fluorescence spectra at each map pixel with sufficient dwell times to permit measurement of minor elements at relatively low abundances (femtogram levels). Fe has been used, with good reason, as the marker for cometary material by the majority of synchrotron microprobe groups studying Stardust. Although the X-ray microprobe measurements cannot measure many low Z elements, including Si and O due to aerogel backgrounds and Al, Mg, and C due to strong absorption, microscopy studies have shown that fine beads of Fe-sulfides are commonly distributed down impact tracks and associated with particles. In this manner, Fe elemental maps are generally good means of locating comet debris in aerogel. Elemental maps in other elements have also been generated and show some spatial variation in composition within individual impact tracks.

The Stardust aerogel is unfortunately contaminated with elements of interest in the comet itself including Fe, Ca, Zn, and Cu and possibly Br. As a result, separation of aerogel and cometary material is important for accuracy and sensitivity of composition measurements. Applying a simple threshold to the Fe fluorescence signal to sort map pixels into cometary material and aerogel background categories carries the risk of greatly underestimating the abundances of minor elements.

We have presented a dual threshold approach in which a safety margin is established and those pixels falling within it are discarded. This provides more accurate composition results without significant loss of cometary material in the analysis. Analyses of Track 12 by both single and dual threshold approaches show the potential impact on mass abundances. 13% more total mass was measured by dual threshold analysis with increases of 1.4× in Cr and Mn mass, 2× in Cu, As, and K, and 4× in Zn. As expected, high abundance elements, Fe and Ni, are not impacted significantly. The dual threshold approach has proven to be a useful diagnostic tool for detecting elements not strongly associated with Fe. Additional cometary Cr in Track 12 was located in this manner.

The dual threshold analysis also reveals contamination: Au contamination sometimes seen intimately associated with cometary material in Stardust impact tracks has been excluded from cometary material composition results because it has been found to be a localized surface Au contaminant occasionally impacted by comet dust and carried down an impact track. The dual threshold technique can be used in other similar situations where elements of interest in a small sample embedded in a matrix are also present in the matrix itself.

We have presented the refined whole impact track and terminal particle compositions by mass and by atoms for each of the five Stardust impact tracks. Compositions for all tracks except Track 5, which has unusually high levels of background contamination, were generated using the dual threshold method. A total of about 3.8 nanograms of Fe mass was measured in these five impact tracks. From the limited sample analyzed thus far, we find that terminal particles in conical tracks tend to contain large percentages of the total mass in the terminal particle while those in bulbous tracks contain less. Based on whole impact track and terminal particle compositions, educated guesses of the dominant minerals present in the impact track and/or terminal particle have been made.

The composition results presented here will be combined in the future with additional data to better constrain the bulk composition of the comet 81P/Wild 2 sample. Improved accuracy analyses like the dual threshold approach will become critical to narrowing the uncertainty levels on the bulk composition as the number of analyzed impact tracks increases and the limited number of samples no longer dominates the uncertainty. X-ray microprobe studies will continue to play a major role in non-destructive analysis to better understand the effects of impact on the original impacting dust and component minerals both by fluorescence and X-ray absorption spectroscopy. Unraveling the complex interactions and relationships between collection media, contaminants and comet dust will be a major theme for future Stardust research.

Acknowledgments—This manuscript benefited greatly from the insightful comments of Steve Sutton, Thomas Stephan, and Donald Brownlee. We gratefully acknowledge NASA and the Stardust Preliminary Examination Teams for the opportunity to study such exciting and unique samples. We also thank the Bulk Chemistry Subteam for useful interactions and discussions, and we acknowledge the

enormous efforts of all involved in curation to carry out rapid sample preparation and distribution. Portions of this work were carried out at the Stanford Synchrotron Radiation Laboratory, a national user facility operated by Stanford University on behalf of the U.S. Department of Energy, Office of Basic Energy Sciences. This work was performed in part under the auspices of the U.S. Department of Energy, National Nuclear Security Administration by the University of California, Lawrence Livermore National Laboratory, contract No. W-7405-Eng-48. This work was supported by NASA Grants NNH06AD67I (Stardust Participating Scientist) and NNH04AB49I (SRLIDAP).

Editorial Handling—Dr. Donald Brownlee

REFERENCES

Brownlee D. E., Tsou P., Anderson J. D., Hanner M. S., Newburn R. L., Sekanina Z., Clark B. C., Hörz F., Zolensky M. E., Kissel J., McDonnell J. A. M., Sandford S. A., and Tuzzolino A. J. 2003. Stardust: Comet and interstellar dust sample return mission. *Journal of Geophysical Research* 108:SRD 1-1–1-15.

Brownlee D. E., Tsou P., Burnett D., Clark B., Hanner M. S., Hörz F., Kissel J., McDonnell J. A. M., Newburn R. L., Sandford S., Sekanina Z., Tuzzolino A. J., and Zolensky M. 2006a. The Stardust mission: Returning comet samples to Earth (abstract #2286). 37th Lunar and Planetary Science Conference. CD-ROM.

Brownlee D., Tsou P., Aléon J., Alexander C. M. O'D., Araki T., Bajt S., Baratta G. A., Bastien R., Bland P., Bleuet P., Borg J., Bradley J. P., Brearley A., Brenker F., Brennan S., Bridges J. C. Browning N., Brucato J. R., Brucato H., Bullock E., Burchell M. J., Busemann H., Butterworth A., Chaussidon M., Cheuvront A., Chi M., Cintala M. J, Clark B. C., Clemett S. J., Cody G., Colangeli L., Cooper G., Cordier P. G., Daghlian, C., Dai Z., D'Hendecourt L., Djouadi Z., Dominguez G., Duxbury T., Dworkin J. P., Ebel D., Economou T. E., Fairey S. A. J., Fallon S., Ferrini G., Ferroir T., Fleckenstein H., Floss C., Flynn G., Franchi I. A., Fries M., Gainsforth Z., Gallien J.-P., Genge M., Gilles M. K., Gillet P., Gilmour J., Glavin D. P., Gounelle M., Grady M. M., Graham G. A., Grant P. G., Green S. F., Grossemy F., Grossman L., Grossman J., Guan Y., Hagiya K., Harvey R., Heck P., Herzog G. F., Hoppe P., Hörz F., Huth J., Hutcheon I. D., Ishii H., Ito M., Jacob D., Jacobsen C., Jacobsen S., Joswiak D., Kearsley A. T., Keller L., Khodja H., Kilcoyne A. L. D., Kissel J., Krot A., Langenhorst F., Lanzirotti A., Le L., Leshin L., Leitner J., Lemelle L., Leroux H., Liu M.-C., Luening K., Lyon I., MacPherson G., Marcus M. A., Marhas K., Matrajt G., Meibom A., Mennella V., Messenger K., Mikouchi T., Mostefaoui S., Nakamura T., Nakano T., Newville M., Nittler L. R., Ohnishi I., Ohsumi K., Okudaira K., Papanastassiou D. A., Palma R., Palumbo M. O., Pepin R. E., Perkins D., Perronnet M., Pianetta P., Rao W., Rietmeijer F., Robert F., Rost D., Rotundi A., Ryan R., Sandford S. A., Schwandt C. S., See T. H., Schlutter D., Sheffield-Parker J. A., Simionovici S., Sitnitsky S. I., Snead C. J., Spencer M. K., Stadermann F. J., Steele A., Stephan T., Stroud R., Susini J.,. Sutton S. R., Taheri M., Taylor S., Teslich N., Tomeoka K., Tomioka N., Toppani A., Trigo-Rodríguez J. M., Troadec D., Tsuchiyama A., Tuzolino A. J., Tyliszczak, T., Uesugi K., Velbel M., Vellenga J., Vicenzi E., Vincze L., Warren J., Weber I., Weisberg M., Westphal A. J., Wirick S., Wooden D., Wopenka B., Wozniakiewicz P. A., Wright I., Yabuta H., Yano H., Young E. D., Zare R. N., Zega T., Ziegler K., Zimmerman L., Zinner E., and Zolensky M. 2006. Comet Wild 2 under a microscope. *Science* 314:1711–1716.

Flynn G., Bleuet P., Borg J., Bradley J. P., Brenker F., Brennan S., Bridges J. C. Brownlee D. E., Bullock E., Burghammer M., Clark B. C., Dai Z. R., Daghlian C. P., Djouadi Z., Fakra S., Ferroir T., Floss C., Franchi I. A., Gainsforth Z., Gallien J.-P., Gillet P., Grant P. G., Graham G. A., Grossemy F., Heck P., Herzog G. F., Hoppe P., Hörz F., Huth J., Igantyev K., Ishii H., Janssens K., Joswiak D., Kearsley A. T., Khodja H., Lanzirotti A., Leitner J., Lemelle L., Leroux H., Luening K., MacPherson G., Marhas K., Matrajt G., Nakamura T., Nakamura-Messenger K., Nakano T., Newville M., Papanastassiou D. A., Pianetta P., Rao W., Riekel C., Rietmeijer F., Rost D., Schwandt C. S., See T. H., Sheffield-Parker J. A., Simionovici S., Sitnitsky S. I., Snead C. J., Stadermann F. J., Stephan T., Stroud R. M., Susini J., Suzuki Y., Sutton S. R., Taylor S., Teslich N., Troadec D., Tsou P., Tsuchiyama A., Uesugi K., Vekemans B., Vicenzi E., Vincze L., Westphal A. J., Wozniakiewicz P. A., Zinner E., and Zolensky M. 2006. Elemental compositions of comet 81P/Wild 2 samples collected by Stardust. *Science* 314: 1731–1735, and supporting online material.

Hörz F., Bastien, R., Borg J., Bradley, J. P., Bridges J. C., Brownlee D. E., Burchell M. J., Cintala M. J., Dai Z. R., Djouadi Z., Dominguez G., Economou T. E., Fairey S. A. J., Floss C., Franchi I. A., Graham G. A., Green S. F., Heck H., Hoppe P., Huth J., Ishii H., Kearsley A. T., Kissel J., Leitner J., Leroux H., Marhas M., Messenger K., Schwandt C. S., See T. H., Snead S., Stadermann F. J., Stephan T., Stroud R., Teslich N., Trigo-Rodríguez J. M., Tuzzolino A. J., Troadec D., Tsou P., Warren J., Westphal A., Wozniakiewicz P. J., Wright I., and Zinner E. 2006. Impact features on Stardust: Implications for comet Wild 2 dust. *Science* 314:1716–1719.

Irvine W. M. and Lunine J. I. 2004. The cycle of matter in our galaxy: From clouds to comets. In *Comets II*, edited by Festou M. C., Keller H. U., and Weaver H. A. Tucson, Arizona: The University of Arizona Press. pp. 25–31.

Jessberger E. K. 1999. Rocky cometary particulates: Their elemental, isotopic, and mineralogical ingredients. *Space Science Reviews* 90:91–97.

Keller L. P., Bajt S., Baratta G. A., Borg J, Bradley J. P., Brownlee D. E., Busemann H., Brucato J. R., Burchell M., Colangeli L., D'Hendecourt L., Djouadi Z., Ferrini G., Flynn G., Franchi I. A., Fries M., Grady M. M., Graham G. A., Grossemy F., Kearsley A., Matrajt G., Nakamura-Messenger K., Mennella V., Nittler L., Palumbo M. E., Stadermann F. J., Tsou P., Rotundi A., Sandford S. A., Snead C., Steele A., Wooden D., and Zolensky Z. 2006. Infrared spectroscopy of comet 81P/Wild 2 samples returned by Stardust. *Science* 314:1728–1731.

Królikowska M. and Szutowicz S. 2006. Non-gravitational motion of the Jupiter-family comet 81P/Wild 2. I. The dynamical evolution. *Astronomy & Astrophysics* 448:401–409.

Lodders K. 2003. Solar system abundances and condensation temperatures of the elements. *The Astrophysical Journal* 591: 1220–1247.

McKeegan K. D., Aléon J., Bradley J., Brownlee D., Busemann H., Butterworth A., Chaussidon M., Fallon S., Floss C., Gilmour J., Gounelle M., Graham G., Guan Y., Heck P. R., Hoppe P., Hutcheon I. D., Huth J., Ishii H., Ito M., Jacobsen S. B., Kearsley A., Leshin L. A., Liu M.-C., Lyon I., Marhas K., Marty B., Matrajt G., Meibom A., Messenger S., Mostefaoui S., Mukhopadhyay S., Nakamura-Messenger K., Nittler L., Palma R., Pepin R. O., Papanastassiou D. A., Robert F., Schlutter D., Snead C. J., Stadermann F. J., Stroud R., Tsou P., Westphal A., Young E. D., Ziegler K., Zimmermann L., and

Zinner E. 2006. Isotopic compositions of cometary matter returned by Stardust. *Science* 314:1724–1727.

Sandford S. A., Aléon J., Alexander C. M. O.'D., Araki T., Bajt S., Baratta G. A., Borg J., Bradley J. P., Brownlee D. E., Brucato J. R., Burchell M. J., Busemann H., Butterworth A., Clemett S. J., Cody G., Colangeli L., Cooper G., D'Hendecourt L., Djouadi Z., Dworkin J. P., Ferrini G., Fleckenstein H., Flynn G. J., Franchi I. A., Fries M., Gilles M. K., Glavin D. P., Gounelle M., Grossemy F., Jacobsen C., Keller L. P., Kilcoyne A. L. D., Leitner J., Matrajt G., Meibom A., Mennella V., Mostefaoui S., Nittler L. R., Palumbo M. E., Papanastassiou D. A., Robert F., Rotundi A., Snead C. J., Spencer M. K., Stadermann F. J., Steele, A., Stephan T., Tsou P., Tyliszczak T., Westphal A. J., Wirick S., Wopenka B., Yabuta H., Zare R. N., and Zolensky M. E. 2006. Organics captured from the comet Wild 2 by the Stardust spacecraft. *Science* 314:1720–1724.

Sekanina Z. and Yeomans D. K. 1985. Orbital motion, nucleus precession, and splitting of periodic comet Brooks 2. *The Astronomical Journal* 90:2335–2352.

Solé V. A., Papillon E., Cotte M., Walter Ph., and Susini J. 2007. A multiplatform code for the analysis of energy-dispersive X-ray fluorescence spectra. *Spectrochimica Acta B* 62:63–68. The code is available online at http://www.esrf.fr/computing/bliss/downloads/index.html.

Tsou P., Brownlee D. E., Sandford S. A., Hörz F., and Zolensky M. E. 2003. Wild 2 and interstellar sample collection and Earth return. *Journal of Geophysical Research* 108:SRD 3-1–21.

Westphal A. J., Snead C., Butterworth A., Graham G. A., Bradley J. P., Bajt S., Grant P. G., Bench G., Brennan S., and Pianetta P. 2004. Aerogel keystones: Extraction of complete hypervelocity impact events from aerogel collectors. *Meteoritics & Planetary Science* 39:1375–1386.

Zolensky M. E., Zega T. J., Yano H., Wirick S., Westphal A. J., Weisberg M. K., Weber I., Warren J. L., Velbel M. A., Tsuchiyama A., Tsou P., Toppani A., Tomioka N., Tomeoka K., Teslich N., Taheri M., Susini J., Stroud R., Stephan T., Stadermann F. J., Snead C. J., Simon S. B., Simionovici A., See T. H., Robert F., Rietmeijer F. J. M., Rao W., Perronnet M. C., Papanastassiou D. A., Okudaira K., Ohsumi K., Ohnishi I., Nakamura-Messenger K., Nakamura T., Mostefaoui S., Mikouchi T., Meibom A., Matrajt G., Marcus M. A., Leroux H., Le Melle L., Le L., Lanzirotti A., Langenhorst F., Krot A. N., Keller L. P., Kearsley A. T., Joswiak D., Jacob D., Ishii H., Harvey R., Hagiya K., Grossman L., Grossman J. N., Graham G. A., Gounelle M., Gillet P., Genge M. J., Flynn G., Ferroir T., Fallon S., Ebel D. S., Dai Z. R., Cordier P., Clark B., Chi M., Butterworth A. L., Brownlee D. E., Bridges J. C., Brennan S., Brearley A., Bradley J. P., Bleuet P., Bland P. A., and Bastien R. 2006. Mineralogy and petrology of comet 81P/Wild 2 nucleus samples. *Science* 314:1735–1739.